Electronic Supplementary Material (ESI) for Physical Chemistry Chemical Physics.

Size and shape dependency of surface energy of metallic nanoparticles: Unifying the atomic and thermodynamic approach

Bastiaan Molleman and Tjisse Hiemstra

Electronic Supplementary Information
(16 pages, 4 figures, 3 tables)

*Corresponding author' s email address: **bastiaan.molleman@wur.nl**
Department of Soil Quality, Wageningen University
P.O. Box 47, 6700 AA Wageningen, the Netherlands

S1 Edge and corner contributions

As we discuss in the main text, cylindrical and spherical geometry is used to calculate the surface area contribution of edges and corners, respectively. We imagine the surface plane as lying on the surface of the atoms, which are considered as hard spheres with a diameter equal to the closest interatomic distance (d_a) in the crystal lattice.

Surface area contribution of edges

When two surfaces meet at an angle, an edge is formed, as is shown in Figure S1 (left panel). In our approach, the edge that connects two surfaces is taken to be a section of a cylinder, which fits exactly over the outermost surface of the edge atoms. The top and the bottom of this cylinder are formed by great circles on the corner atoms, perpendicular to both connecting surfaces. The length of the cylinder is thus equal to the distance between the cores of the corner atoms, i.e. $l = d_a(s - 1)$, where d_a is the interatomic distance and s is the number of atoms in an edge, including the two corner atoms.

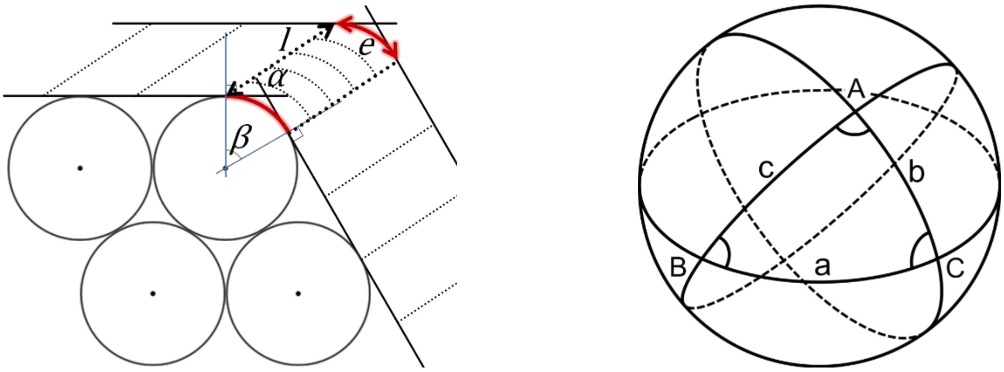

Figure S1. Surface area contribution of edges and corners. The left panel shows a cross-section of an idealised edge, with the shells and cores of atoms in black. The curved surface in between the thick dotted lines and the red curves, which is attributed to the edge has an area of $e \cdot l$. The dihedral angle α is the angle between facets; β is needed for the length of e. The right panel shows a sphere with three great circles, enclosing the spherical triangle ABC, with internal angles ABC, ACB, and BAC. For a spherical triangle, the spherical excess is equal to $\Delta = \angle ABC + \angle ACB + \angle BAC - \pi$.

A facet ends where the surface is tangent with the shells of the atoms of the edge. Only the section of the cylinder that stretches between the two facets contributes to the surface area. If we call the length of the section e, then the cylindrical section has an area equal to $e \cdot l$. The length of e is determined by the dihedral angle α. As we see in the figure, the length of the red section is equal to $\beta \cdot r$, if β is in rad. From the figure, we can tell that $\beta = 2\pi - 2 \cdot ½\pi - \alpha = \pi - \alpha$; if, in addition, $r = ½d_a$, then the total surface area of the edge can be given as: $e \cdot l = ½d_a^2(\pi - \alpha)(s - 1)$.

Surface area contribution of corners

A corner atom connects to several edges. It thus has several great circles around it, which from the bottom-circles of the edge cylinders. This leaves a spherical polygon on the shell of the corner atom, which is not covered by the surface area attributed to the edges or the planes. A spherical triangle is shown as an example in the right panel of Figure S1.

The surface area of a spherical polygon, which we attribute to the corner, follows from the spherical excess (Δ), according to $r^2\Delta$.[1] The spherical excess follows from the sum of the internal angles ($\sum\theta_k$) and the number of corners in the polygon (p), according to $\Delta = \sum\theta_k - \pi\,(p - 2)$. The internal angles ($\theta_\mathrm{k}$) of the spherical polygon on the corner atoms, which is formed by the great circles perpendicular to the adjoining edges, follow from the angles between these edges (η_k) in the same way that β follows from α (see above), i.e. $\theta = \pi - \eta$. It follows that $\sum\theta_k = p\pi - \sum\eta_k$ and the spherical excess can thus be expressed as $\Delta = 2\pi - \sum\eta_k$. The area of a corner is thus equal to $\frac{1}{4}d_\mathrm{a}^2(2\pi - \sum\eta_k)$

The angles between edges η are readily observed from the surface facets, and are limited to ½π, ⅓π, and ⅔π for square, triangular, and hexagonal facets respectively. An overview is given in Table S1. Interestingly, the summed contribution of all corners of geometrically shaped particles treated here is invariably equal to $d_\mathrm{a}^2\pi$.

Table S1. Overview of geometrical properties of corner atoms on regularly shaped particles in the FCC crystal lattice.

Particle geometry	z_j[a]	[111]▲[b] $\eta = \frac{1}{3}\pi$	[111]⬣[b] $\eta = \frac{2}{3}\pi$	[100]■[b] $\eta = \frac{1}{2}\pi$	Δ[c]
Icosahedron	12	5			$^1/_3\,\pi$
Truncated decahedron	2	5			$^1/_3\,\pi$
	10	2		2	$^1/_3\,\pi$
Octahedron	6	4			$^2/_3\,\pi$
Cuboctahedron	12	2		2	$^1/_3\,\pi$
Truncated octahedron	24		2	1	$^1/_6\,\pi$

[a] Number of times the jth corner is found in a particular particle geometry

[b] Number of facets connecting at a corner, where η is the angel between the sides of a triangular (▲) or hexagonal (⬣) [111] facet, or a square (■) [100] facet.

[c] Spherical excess calculated using $\Delta = \sum\theta_k - \pi\,(p - 2)$, with p = [111]▲+ [111]⬣ + [100]■ or using $\Delta = 2\pi - \sum\eta_k$

S2 Tolman for non-spherical particles

The classical Tolman equation has been derived for spherical particles, however, an adapted version for faceted and spheroidal particles can be obtained with relative ease. To demonstrate this, we will first consider a number of crucial steps in the derivation of the Tolman equation.

An important intermediate result in the derivation of the Tolman equation is that the change in surface tension is proportional to the change in pressure difference between the two phases, according to:[2]

$$d\gamma = -\frac{\Gamma}{\rho_1 - \rho_2} d(p_1 - p_2) \qquad (S1)$$

in which γ is the surface tension (J m^{-2}), Γ is the excess adsorption (mol m^{-3}), and ρ_1 and ρ_2 are the bulk densities (mol m^{-3}) in the first and the second phase considered, respectively, while p_1 and p_2 are the pressures (J m^{-3}) in said phases.

Using the Laplace equation, the pressure difference is expressed in terms of surface tension γ and radius r ($p_1 - p_2 = 2\gamma/r$), leading to:

$$d\gamma = -\frac{\Gamma}{\rho_1 - \rho_2} d\left(\frac{2\gamma}{r}\right) \qquad (S2)$$

If the term $\Gamma/(\rho_1 - \rho_2)$ is equated to the Tolman length δ (which is valid as long as $\delta << r$), the above equation can be solved to yield the Tolman equation in the well-known form given in the main text (eq 6).[2]

The Laplace equation

Spherical particles. The Laplace equation in its traditional form is valid for spherical particles. There are several ways to derive the Laplace equation. According to one of the described derivations,[3] the Laplace equation can be written as:

$$p_1 - p_2 = \gamma \frac{dA}{dV} \qquad (S3)$$

The difference in pressure depends on the change of surface area (dA) with change of volume (dV) at a given surface tension γ. In the above equation, the derivatives dA and dV can be related to the radius r of a spherical particle, i.e. dA/dr and dV/dr, and with $A = 4\pi r^2$ and $V = 4/3\cdot\pi r^3$, the traditional formulation of the Laplace equation can be obtained.

Facetted particles. In our approach, Laplace expressions for non-spherical faceted particles, will be obtained by expressing surface area as a function of an equivalent radius. For this, we use the relationship between surface area and volume, which is well-defined for faceted particles. Formulae for surface area and volume, as a function of edge-length l, are given in Table S2 for selected particle geometries.

Table S2. Surface area and volume of a selection of faceted particles as a function of edge-length *l*.

Particle geometry	Surface area	Volume	c[a]
Cuboctahedron	$(6+2\sqrt{3})l^2$	$\frac{5}{3}\sqrt{2}l^3$	1.105
Octahedron	$2\sqrt{3}l^2$	$\frac{1}{3}\sqrt{2}l^3$	1.183
Truncated octahedron	$(6+12\sqrt{3})l$	$8\sqrt{2}l^3$	1.099
Icosahedron	$(5\sqrt{3})l^2$	$\frac{5}{12}(3+\sqrt{5})l^3$	1.065
Truncated decahedron	$\left(5+\frac{5}{2}\sqrt{3}\right)a^2$	$\frac{5}{4}\sqrt{5+2\sqrt{5}}\left(1+\frac{2}{3}\sqrt{1-\frac{2}{5-\sqrt{5}}}\right)a^3$	1.100

[a] Ratio between surface area of the faceted particle and a spherical particle of equal volume

Oblate and prolate spheroids. For spheroidal particle, a similar shape factor can be established. The surface area for oblate and prolate spheroids with an equatorial radius *a* and a polar radius *b* can be calculated using the following equations:

$$A_{oblate} = 2\pi a^2 + \frac{2\pi b^2}{\sqrt{1-b^2/a^2}} \cdot arctanh\left(\sqrt{1-\frac{b^2}{a^2}}\right) \qquad (S4a)$$

$$A_{prolate} = 2\pi a^2 + \frac{2\pi ab}{\sqrt{1-a^2/b^2}} \cdot arcsin\left(\sqrt{1-\frac{a^2}{b^2}}\right) \qquad (S4b)$$

The volume for both types of spheroidal particles is equal to $4/3 \cdot \pi a^2 b$. Using the above formulae, a shape factor can be coupled to the ratio between the equatorial and the polar radius *a/b*. This is shown in Figure S2.

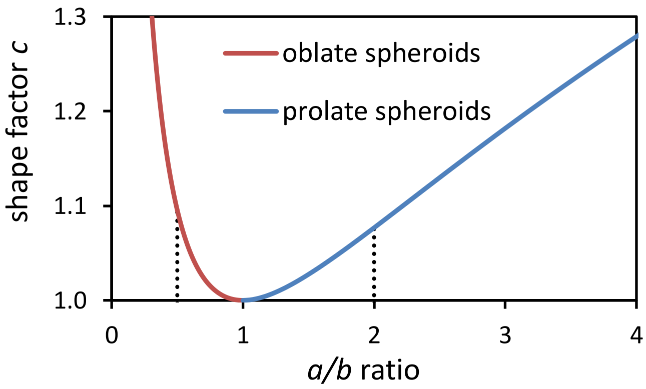

Figure S2. Shape factor *c* for oblate and prolate spheroidal particles, plotted against the ratio *a/b* between the equatorial and polar axis. Below a ratio of 1 particles are oblate, above they are prolate. The vertical dotted lines are positioned at *a/b* ratios of 0.5 and 2, we expect that most nanoparticle particles will fall in between these limits.

Generalized Tolman equation

Using the shape factor c, the Laplace equation for faceted and spheroidal particles becomes $\Delta p = 2c\gamma/r$. This adapted Laplace equation can be readily used in the derivation of the Tolman equation, leading to:

$$\gamma_r = \frac{\gamma_\infty}{1 + 2c\delta/r_s} = \gamma_\infty \left(1 + \frac{2c\delta}{r_e - \delta}\right)^{-1} \qquad (S5)$$

The effect of the introduction of c in the Tolman equation depends on the value of the Tolman length and the particle size. For the Tolman lengths that we derived for metallic nanoparticles in this work, the effects are very limited for particles larger than ~2 nm as shown in Figure S3.

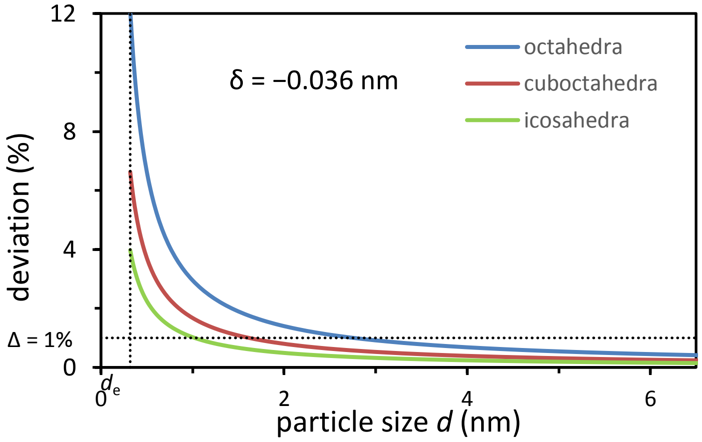

Figure S3. The deviation (%) of the adapted Tolman equation (eq S4) from the classical Tolman equation (eq 6) for octahedral, cuboctahedral, and icosahedral particles (from top to bottom). The lines are calculated using a Tolman length of −0.036 nm, which is the value that we will later establish for cuboctahedral gold nanoparticles (see Results and Discussion). The horizontal dotted represents a deviation of 1%; the vertical dotted line represents the equimolar diameter d_e for a single gold atom, calculated using equation 1 (main text).

Concluding remarks

Above we have treated shapes with sharp corners and edges. However, the physical surface area that we formulate in this work explicitly includes the surface area of rounded edges end corners. Given the limited difference between a spherical Tolman approach and a faceted Tolman approach, we feel that such details can be left untreated.

We are also aware, if the surface of tension is located at a uniform distance from the equimolar surface, their geometries are not necessarily identical for non-spherical particles. This is the case for cuboctahedra, truncated octahedra and truncated decahedra, as well as for oblate and prolate particles. For applications of equation S5 in this work, the shape change is minor. However, for very small, non-spherical water droplets, this may be relevant.

S3 How surface energy depends on the radius of tension

In the main text we explain that upon choosing a radius of tension r_S, a surface energy value can be calculated in two ways. Thermodynamically, using the Tolman equation, and atomically, by scaling the excess particle energy to the surface area. Crucial for determining the position of the surface of tension is that both calculated surface energy values depend differently on the chosen value for the radius of tension r_S. This is illustrated in Figure S4. Because of the opposite dependence on r_S, the calculated lines intersect; this is universally seen. The true radius of tension r_S and size-dependent surface energy γ_r are found where the lines intersect, i.e. at the r_S value where both methods yield the same surface energy.

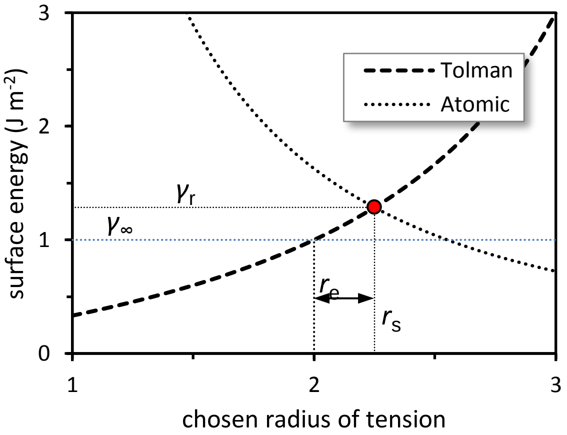

Figure S4. Relation between surface energy and the radius of tension r_S for the thermodynamic (dashed line) and the atomic (dotted line) method of calculating surface energy. Lines have been calculated for a spherical particle with an equimolar radius r_e of 2 nm, and an excess particle energy ΔE_S of 81.8 aJ. The consistent value of r_S and the corresponding surface energy γ_r are found where the lines cross, as indicated with a red dot. Also indicated is the planar surface energy, γ_∞. The difference between r_e and r_S is the Tolman length given with the horizontal arrow.

S4 Nucleation of water cavities

Very recently, the nucleation of cavities in water has been studied with state-of-the-art advanced MD simulations.[4] The Gibbs free energy of formation of cavities in water was calculated as a function of cavity size for negative pressures p in the range of −100 to −200 MPa. These simulated Gibbs free energy curves are given in Figure S5 with symbols. If the cavity volume is very small, energy is needed to enlarge it, while for large volumes, Gibbs free energy is released at enlargement of the cavity. In the latter case, the cavity can grow spontaneously. However, if the cavity is smaller than a critical value, it may spontaneously collapse. On the top of the energy barrier, the critical particle is in an instable state.

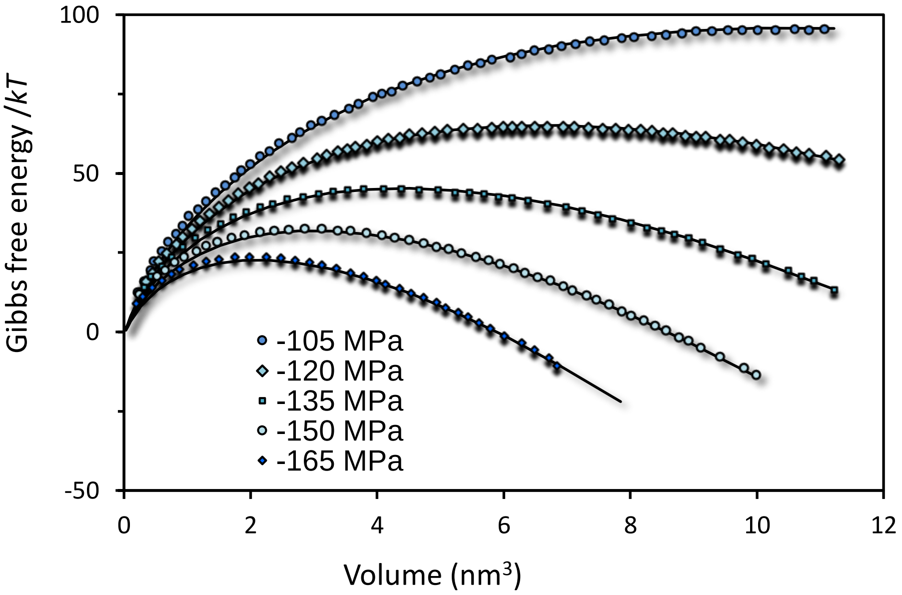

Figure S5. Gibbs free energy of cavity formation in water as a function of the equimolar cavity diameter for various values for the applied negative pressure. The symbols are values of Menzl et al.[4] that were obtained with advanced MD simulations. The lines have been calculated with homogeneous nucleation theory using a size-dependent surface tension (eq S6) according to the Tolman approach with a mean shape fatcor of c = 1.1 (see text). The curves were calculated using the Tolman length as the only adjustable parameter leading to $\delta = 0.067$ nm.

The generated MD data have been described by Menzl et al.[4] with classical nucleation theory allowing the surface tension to be size-dependent by introducing a Tolman length.[4] The authors applied an expression that is based on the surface of tension with corresponding radius (r_s), whereas in their data treatment, the calculated radius is based on the equimolar volume, making it equivalent to r_e. This principal difference is the cornerstone of the thermodynamic treatment of Tolman. It implies that the radius in their expressions is to be replaced by $r_e - \delta$, where appropriate. The proper expression to be applied in critical nucleation theory is:

$$\Delta G(r_e) = 4\pi c (r_e - \delta)^2 \frac{\gamma_\infty}{1 + 2c\delta/(r_e - \delta)} + \frac{4\pi r_e^3}{3} p \qquad (S6)$$

in which *c* is the shape factor for deviation from the perfect sphere. In equation S5, the first term gives the contribution of surface Gibbs free energy and the second term gives the contribution of the formation of the water cavity.

A second point is that Menzl et al.[4] have made the surface tension γ_∞ of water in the planar limit to an adjustable parameter, in order to get an excellent fit. However, it leads to a significantly higher value for the surface tension γ_∞ of water than found experimentally. Considering the planar surface tension of water γ_∞ as an adjustable parameter is doubtful since it may be assume that the advanced MD model applied is able to reproduce the experimental value correctly.

In Figure S5, the given lines have been calculated with the above expression for homogeneous nucleation. In our treatment of their data, a good fit could not be achieved when the Tolman length δ is considered as the only adjustable parameter. The simulation experiments of Menzl et al.[4] showed that the particles shape is non-spherical. If the shape factor *c* is introduced and used as an adjustable parameter, an excellent fit is found for the full data set, with only minor deviations, as is shown in Figure S5. The data is best described with a size independent shape factor of $c = 1.1$ and $\delta = +0.067$ nm. The Tolman length is much lower than the high value found by Menzl et al.[4] ($\delta = +0.195$ nm) and closer to the value estimated by Tolman $\delta = 0.1$ nm for spherical water droplets and recently found with simulations ($\delta \sim +0.05$-0.10 nm).[5]

The same shape factor is taken for all sizes. Menzl et al.,[4] showed that the particles vary in shape, and in addition, the surfaces of the droplets are quite irregular. By extracting the surface areas and volumes from the MD results, one may in principle calculate the shape factors involved. However, this is beyond the scope of the present paper.

S5 Equimolar surface and Tolman lengths

The equimolar surface

The equimolar surface is defined as the surface within which all the mass would be located in case of a uniform density up to the equimolar surface. While this is fairly straightforward for spherical particles, it is less so for crystalline particles with a polyhedral shape. Rather than establishing an equimolar radius, we will establish a position of the equimolar radius with respect to the center of the surface atoms.

We assume that the mass of an atom is distributed homogeneously within the atomic radius, which we define as half the interatomic distance, i.e. $r_a = ½ d_a$. Figure 4 (main text) shows that atoms in the crystal structure overlap. At the surface, the density is thus lower. It follows that the equimolar surface is located between the cores and the outer shell of surface atoms.

The equimolar surface is located such that the missing sections between surface atoms can be exactly filled in with the sections extending over the equimolar surface. The red dotted lines in Figure 4 of the main text are located exactly between atomic layers, and the overlapping sections from different layers (colored) have exactly the same size. The exact location of the equimolar surface thus follows from the distance between atomic layers.

From the atomic positioning in the FCC lattice, it may be calculated that the distance between [100] and [111] planes is equal to $\sqrt{½}\ d_a$, and $\sqrt{⅔}\ d_a$, respectively. The equimolar surface is located at half that distance, i.e. $\sqrt{½}\ r_a$, and $\sqrt{⅔}\ r_a$, from the centers of surface atoms.

Specific Tolman lengths for crystal faces

Above we have defined the position of the equimolar surface relative to the centers of surface atoms. In a similar fashion, we can calculate the positions of the surfaces of tension will also be defined, we can calculate the Tolman length.

In our definition, the physical surface (see Figure 2c, main text) is placed on top of the outer shells of surface atoms. In other words, the physical surface is located at a distance of r_a from the centers of surface atoms. This leads to a Tolman length of $(\sqrt{½} - 1)\ r_a$ for the [100] face and $(\sqrt{⅔} - 1)\ r_a$ for the [111] face, leading to $\delta_{100} = -0.146\ d_a$ and $\delta_{111} = -0.092\ d_a$.

Method A (see Figure 2a, main text) places the surface of tension at the center of the surface atoms. Above we have thus given the position of the equimolar surface relative to this surface of tension, leading to $\delta_{100} = 0.354\ d_a$ and $\delta_{111} = 0.408\ d_a$.

For the surface of tension defined in Method B, as given in Figure 2b of the main text, the position is more complex to calculate. Moreover, the location may vary for particles of different shapes, depending on the number of edges. We will here demonstrate the calculation for cuboctahedral particles.

To obtain the distance between the surface of Method B and the center of surface atoms, we calculate the full height of a particle in terms of edge-length (s), which in this method is taken as $s\ d_a$. For a cuboctahedron, the distance between two opposite [100] faces is equal to the diagonal of the [100] face, or $\sqrt{2}\ s\ d_a$. The distance between the cores of two opposite [100] faces is equal to the diagonal of a [100] face defined according to method A, i.e. $\sqrt{2}\ (s - 1)\ d_a$.

It follows that the distance of the surface of tension from method B from the cores is equal to $\frac{1}{2}\sqrt{2}\, d_a$ or $\sqrt{\frac{1}{2}}\, d_a$ at the [100] face.

Using the same principles, though following a much more complicated route, it can be calculated that the distance between the surface of tension and the centers of surface atoms is equal to $\sqrt{\frac{2}{3}} \cdot d_a$ at the [111] face. For cuboctahedra, the Tolman length for the surface of tension defined in method B is thus equal to $\sqrt{\frac{1}{2}}\, r_a - \sqrt{\frac{1}{2}}\, d_a$ for the [100] face and $\sqrt{\frac{2}{3}}\, r_a - \sqrt{\frac{2}{3}}\, d_a$ for the [111] face, leading to $\delta_{100} = -0.354\, d_a$ and $\delta_{111} = -0.408\, d_a$.

S6 Interpretation of additional excess energy data

Size dependency of surface energy of other metallic nanoparticles

In the main text, we identified the physical surface as thermodynamically consistent with the surface of tension. We also showed that with scaling to this surface, the size dependency for surface energy (J m^{-2}) is greatly reduced with respect to trends previously published in literature.[6, 7] A low size-dependency of surface energy is universally observed when computational energy data are scaled to the physical surface area, as shown with additional data in Figure S6, for a variety of particle shapes.

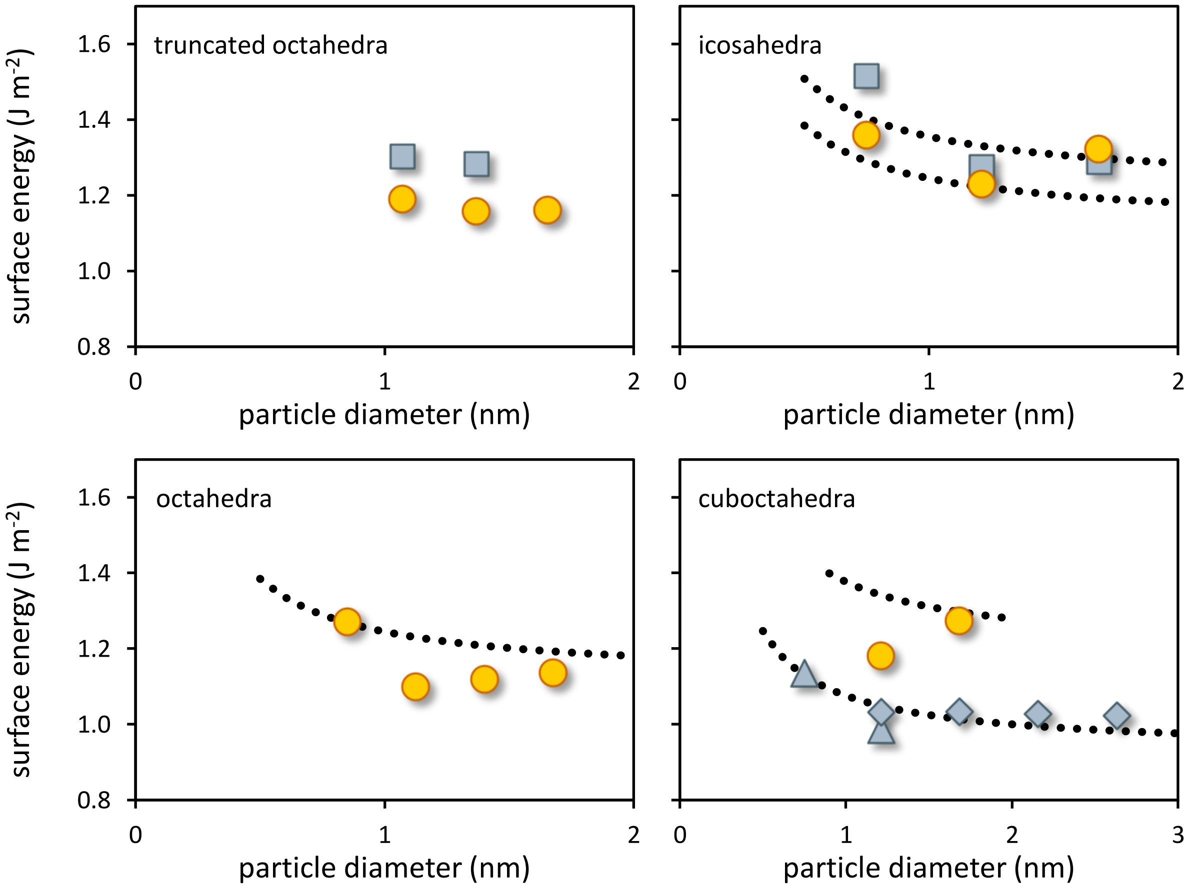

Figure S6. Surface energy data for noble metal nanoclusters in a variety of particle shapes scaled to the physical surface area. Computational data were taken from Liu et al.[8] (DFT-LDA, silver: squares), Barnard and Curtis[9] (DFT-GGA, gold: spheres), Medasani et al.[6] (DFT-GGA, silver: triangles), and Oliveira et al.[10] (SCC-DFTB, silver: diamonds). Tolman functions were generated (dotted lines) using restricted assumptions, which are described below.

Consistency of the physical surface for other metallic nanoparticles

Liu et al.[8] calculated planar surface energies for the silver [111] face and [100] face, being 0.55 and 0.69 eV atom^{-1} respectively. Expressing the surface area of the [111] and [100] face per atom, being respectively 0.072 nm^2 and 0.083 nm^2, yields $\gamma_{[111]}$ = 1.22 J m^{-2} and $\gamma_{[100]}$ = 1.33 J m^{-2}. Using $d_{a,Ag}$ = 0.289[11] and Table S3, we find a surface tension γ_∞ = 1.22 J m^{-2} and a

Tolman length $\delta = -0.027$ nm δ for icosahedral silver clusters. As no macroscopic surface energy data are available in the works by Medasani et al.[6] and Oliveira et al.,[10] a macroscopic surface energy of $\gamma_\infty = 0.93$ J m^{-2} was fitted to the data for silver cuboctahedra.[6, 10]

The model lines for the AuNP have been calculated using a calculated guess of the surface energy for the planar crystal faces $\gamma_{[100]}$ and $\gamma_{[111]}$, as these lack in the paper of Barnard and Curtis.[9] We found that the surface energy of the two silver truncated octahedra with $N = 38$ and $N = 79$ atoms from Liu et al.[8] is between 1.08 and 1.09 times higher than the surface energy of the identically shaped gold truncated octahedra from Barnard and Curtis.[9] Assuming that the same ratio is valid for the planar crystal faces, we get the approximated values of $\gamma_{[100]} = 1.23$ J m^{-2} and $\gamma_{[111]} = 1.12$ J m^{-2} for gold, which we applied. Using $d_{\mathrm{a,Au}} = 0.288$[11] and Table 3, we can generate values for the surface of tension γ_∞ and the Tolman length δ for the different shapes. For icosahedral gold clusters, $\gamma_\infty = 1.12$ J m^{-2} and $\delta = -0.026$ nm; for octahedral gold clusters, $\gamma_\infty = 1.12$ J m^{-2} and $\delta = -0.026$ nm; and for cuboctahedral gold clusters, $\gamma_\infty = 1.19$ J m^{-2} and $\delta = -0.036$ nm.

Overall, the data description by the Tolman equation is good. Individual data points may deviate because of uncertainties in the energy calculation or due to the intricacies in energetics of nanocrystals. Considering the planar surface energy values are the primary input parameter, our method of estimation performs well.

S7 Truncated octahedra

The truncated octahedra shown in Figure 7a of the main text are non-regular, meaning they have two different edge-lengths.[7] As such, these particles are not covered by the general formulas in Table 1 of the main text. We provide dedicated formulae for these particles here.

If s_1 is the number of atoms in the edge between two [111] faces, and s_2 denotes the edge between a [111] and a [100] face, then [111] and [100] facets have the following surface areas:

$$A_{f,[111]} = \sqrt{3}\left((s_1 - 1)(s_2 - 1) + \frac{(s_1 - 1)^2 + (s_2 - 1)^2}{4}\right) \qquad S7a$$

$$A_{f,[100]} = (s_2 - 1)^2 \qquad S7b$$

The surface area of edges and corners can be found using the formulae in Table 1 of the main text.

In the truncated octahedra shown in Figure 7a of the main text, edge-length s_1 was constant with particle size while s_2 increased. It results in a variable surface area ratio of the [100] and the [111] faces, which leads to different values δ and γ_∞. These have been calculated using d_a = 0.288[11] nm and $\gamma_{[111]}$ = 0.79 J m^{-2} and $\gamma_{[100]}$ = 0.92 J m^{-2};[7] values for δ and γ_∞ are given below in Table S3.

Table S3. Edge-lengths, surface area ratios, macroscopic surface energy values and overall Tolman lengths for the truncated octahedra of Figure 7a of the main text.

Edge lengths		$A_{[100]}$ / $A_{[111]}$	γ_∞ (J m^{-2})	δ (nm)
s_1	s_2			
2	3	0.348 / 0.652	0.835	−0.0319
2	5	0.456 / 0.544	0.849	−0.0336
2	7	0.505 / 0.495	0.856	−0.0344
2	9	0.533 / 0.467	0.859	−0.0348
2	11	0.551 / 0.449	0.862	−0.0351

We note that the shape factor c also varies with size for the truncated octahedra described above. The smallest of the above particles is close to a regular truncated octahedron, while the largest rather resembles a cuboctahedron. The shape factor for these particles can thus be expected to be in between those of a regular truncated octahedron and a cuboctahedron. Figure S3 shows that a very limited effect of shape correction is to be expected. It has therefore not been calculated for these particles. Instead, the value for regular truncated octahedra was used in all cases.

S8 Twin plane energy

As we explain, the total surface energy values from Ali et al.[7] include an internal strain contribution due to twinning. The difference between the total surface energy from Ali et al.[7] and the size dependent surface energy can thus be interpreted as twinning energy. The total twinning energy for a cluster (aJ) is found after multiplying the difference (J m^{-2} or aJ nm^{-2}) with the total surface area (nm^2). This value is scaled to the total twin-plane surface area for icosahedra as shown in Figure 8 of the main text.

Icosahedral particles have 30 triangular twin-planes: three shared twin-planes for each of its 20 tetrahedral subunits. The exact definition of the twin-plane for icosahedra can be debated. Two possible surface area definitions are shown in Figure S7; though the resulting twin-plane energy values vary, the trend is not affected by the choice. For our analysis, we use the smaller of the two definitions, indicated by the darker blue in Figure S7.

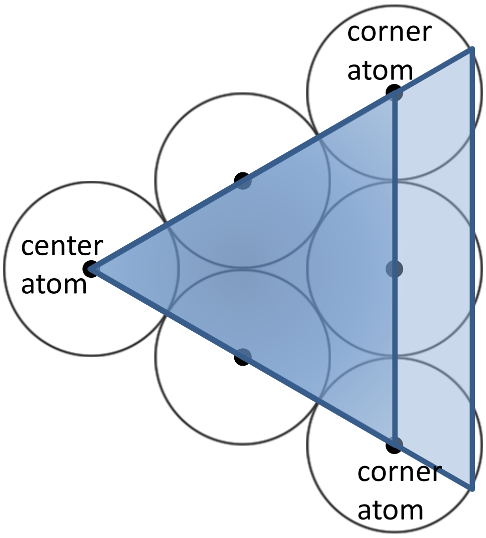

Figure S7. Total twinning energy for icosahedra plotted against twin-plane area. The right panel shows two possible ways of defining the triangulartwin-plane area. There was little difference between the trends found for these two definitions, we have used the smaller of the triangles. In an icosahedron, 30 of these triangular twin-planes are found.

S9 Surface enthalpy

Relating surface enthalpy to the enthalpy of vaporization and atomization

Surface formation can be considered as breaking of intermolecular or interatomic bonds, which requires energy. For a solid or liquid particle, the surface enthalpy contribution to the particle enthalpy is equal to the product $A_p \cdot \Delta H_{surf}$, in which A_p is the specific surface area (m^2 mol^{-1}) and ΔH_{surf} is the surface enthalpy (J m^{-2}). In the simplest approach, the excess surface enthalpy (J mol^{-1}) is calculated assuming a spherical morphology and constant value for ΔH_{surf}. The specific surface area of a particle can be related to the number of atoms N, using the particle radius found according to:

$$A_p = 4\pi r^2 \frac{N_A}{N} = 4\pi \frac{N_A}{N}\left(\frac{3MN}{4\pi N_A \rho}\right)^{2/3} = \left(4\pi \frac{N_A}{N}\right)^{1/3}\left(\frac{3M}{\rho}\right)^{2/3} \qquad (S7)$$

where N_A is Avogadro's number (mol^{-1}), M is the molar mass (g mol^{-1}), and ρ is the bulk density (g m^{-3}). The upper limit of the specific surface area is determined by the radius of a single atom or molecule ($N = 1$).

The result of this approach is given in Figure S8 with full lines for the formation of water nano-droplets and silver nanoparticles. At room temperature, surface enthalpy values (ΔH_{surf}) are respectively 118 mJ m^{-2} for water[12] and 1.52 J m^{-2} for gold (Table 2 main text). These values refer to the slope of the full lines in Figure S8. The value for gold has been derived (next section), using the relationships of Tyson and Miller.[13]

With this simplified approach, the experimental energy of formation of a single molecule or atom in the gas phase is close to the enthalpy of formation (ΔH_f) of the equilibrium phase amended with a surface enthalpy contribution in the size limit. In other words, a major part of the enthalpy of vaporization or atomization is explained by the surface enthalpy that a single liquid molecule or solid atom would have. Introducing a size dependency for the surface enthalpy allows us to close the gap and equate the surface enthalpy of a single molecule or atom formation with the enthalpy of vaporization or atomization, as shown in Figure S8 with dotted lines.

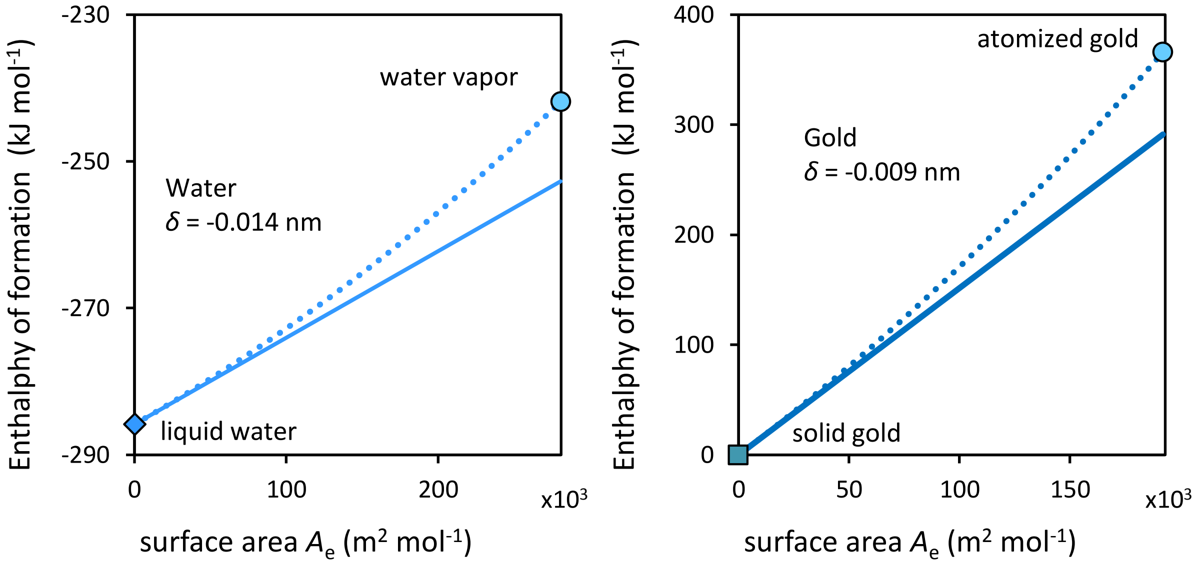

Figure S8. Molar enthalpy of water and gold modified by surface enthalpy, ranging from bulk material to a single molecule or atom. The enthalpy of surface formation for a particle with the size of a single molecule or atom already explains a major part of the enthalpy of evaporation or atomization if a constant surface enthalpy is assumed (solid line). The two values can be unified by introducing size dependency of the surface enthalpy. The uplift of the curve (dotted line) is equivalent with a negative value for the Tolman length.

This size dependency of the surface enthalpy in Figure S8 is obtained using the thermodynamic approach of Tolman (eq 6, main text), applying a Tolman length of $\delta = -0.014$ nm and $\delta = -0.009$ nm, respectively for water and gold. When the same analysis is performed for silver, a Tolman length of -0.006 nm is found. Note that the value for Tolman length of water is for surface enthalpy, and therefore different from the Tolman length in the main text, which is for the surface Gibbs free energy. In case of surface enthalpy, the values for the Tolman length are negative, which is equivalent in Figure S8 with an increase of the slope and an uplift of the curve relating the formation of surface area to the enthalpy change. The diamond and square in Figure S8 are the enthalpy of the bulk liquid and solid, respectively, and the spheres are the enthalpies of the constituting molecule or atom in the gas phase. The difference between both types of values is the enthalpy of vaporization and atomization.

Thermodynamic surface data for gold

While there are ample measurements for the size dependency of surface tension in liquid metals at high temperature, to our knowledge there are none for solid metals. Although the development of computational techniques has created a large body of data, the variation within those data is large. Moreover, the present approach requires a generic single surface energy value, whereas ab initio techniques mostly are applied to specific crystal faces. For this reason, we choose to base ourselves on the only work to date that specifies surface energy for solid metals, based on empirical data.

Tyson and Miller[13] primarily focus on the solid-vapor surface tension, which they estimate to have a value of 1.18 times the liquid-vapor surface tension at the melting temperature (T_M). Using the data available at the time, this correlation leads to a surface tension of 1.33 J m^{-2} for solid gold at $T = T_M$. Using the latest experimental data, [14-16] an average of $\Delta G_{\text{surf, (l)}} = 1.13 \pm 0.02$ J m^{-2} is found for liquid gold at the melting temperature, suggesting a value of $\Delta G_{\text{surf, (s)}} = 1.34$ J m^{-2} for solid gold.

Additionally, Tyson and Miller[13] devoted a section in their paper to surface entropy. In short, they argued that surface entropy is linked to the surface area per mole of surface atoms (A_m), estimated using 1.612 $N_\text{A}^{1/3} V_\text{m}^{2/3}$, where N_A is Avogadro's number and V_m is the molar volume (m^3 mol^{-1}). The entropy contribution is found as the sum of contributions from 3 different temperature intervals (Figure S9). At heating from 0 K to the Debye temperature (T_D), the entropy increases linearly from 0 to 0.8 R/A_m, where R is the gas constant R = 8.134 J mol^{-1} K^{-1}. Between the T_D and ½T_M, the surface entropy is constant at 0.8R/A_M, and between ½T_M and T_M, it increases linearly from 0.8 R/A_M to 1.8 R/A_M.

The surface entropy for solid gold at the melting temperature, as it follows from these relationships (0.23 mJ m^{-2} K^{-1}), exceeds the surface entropy for liquid gold, as found from the temperature dependence of the surface tension (0.15 ± 0.01 mJ m^{-2} K^{-1}).[14-16] We have plotted the temperature dependence of surface entropy[13] for solid gold in Figure S9, using the theoretical value ΔS_surf = 0.23 mJ m^{-2} K^{-1} at $T = T_\text{M}$, a melting temperature of T_M = 1337 K, and $T_\text{D} = 0.2\ T_\text{M}$.

With the above information for solid gold, one is able to calculate the temperature dependency of the surface enthalpy using ΔG_surf = 1.34 J m^{-2} at the melting temperature. The corresponding enthalpy follows from $\Delta H_\text{surf} = \Delta G_\text{surf} + \text{T}\Delta S_\text{surf}$. The temperature dependency of ΔG_surf follows from:[13]

$$\Delta G_{\text{surf}} - \Delta G_{\text{surf}}(T_\text{M}) = \int_{T}^{T_\text{M}} \Delta S_{\text{surf}}\, dT \qquad (S7)$$

The results of these calculations are summarized in Table 2 (main text) and visualized in Figure S9.

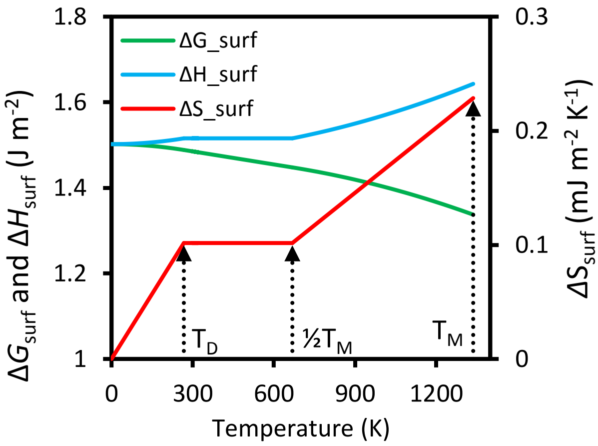

Figure S9. Temperature dependence of surface free energy (ΔG_{surf}) and surface entropy (ΔS_{surf}) according to Tyson and Miller,[13] as well as the surface enthalpy (ΔH_{surf}) that follows from it. Surface free energy and surface enthalpy values correpsond to the primary (left) y-axis, surface entropy to the secondary (right) y-axis. The dotted arrows indicate important temperatures for estimating surface entropy: the Debye temperature ($T_D \approx 0.2 T_M$), half of the melting temperature (½T_M) and the melting temperature (T_M).

Thermodynamic surface data for silver

The above procedure has also been performed for silver. Averaging recent experimental data,[17-19] we obtain a surface Gibbs free energy $\Delta G_{\mathrm{surf,\ (l)}}$ for liquid silver at the melting temperature of 0.934 ± 0.03 J m^{-2}. Using the above discussed energetic difference between the surface of solid and liquid metals at T_M, i.e. $\Delta G_{\mathrm{surf,\ (s)}} = 1.18\ \Delta G_{\mathrm{surf,\ (l)}}$,[13] we find $\Delta G_{\mathrm{surf,\ (s)}} = 1.10$ J m^{-2} at $T = T_M$, in accordance with the value of 1.09 J m^{-2}, given by Tyson and Miller.[13] For the surface entropy for solid silver at the melting temperature, we used $\Delta S_{\mathrm{surf}} = 0.23$ mJ m^{-2} K^{-1}, equal to 1.8 R/A_M.[13] This value corresponds very well with the temperature dependency of the surface tension of molten silver 0.21 ± 0.05 mJ m^{-2} K^{-1}.[17-19] Results are given in Table 4 of the main text.

S10 References

1. I. Todhunter, *Spherical Trigonometry: For the Use of Colleges and Schools*, MacMillan and co., London, 1886.
2. R. C. Tolman, *The journal of chemical physics*, 1949, 17, 333-337.
3. H. Vehkamäki, *Classical nucleation theory in multicomponent systems*, Springer Science & Business Media, 2006.
4. G. Menzl, M. A. Gonzalez, P. Geiger, F. Caupin, J. L. Abascal, C. Valeriani and C. Dellago, *Proceedings of the National Academy of Sciences*, 2016, 113, 13582-13587.
5. M. H. Factorovich, V. Molinero and D. A. Scherlis, *Journal of the American Chemical Society*, 2014, 136, 4508-4514.
6. B. Medasani, Y. H. Park and I. Vasiliev, *Physical Review B*, 2007, 75, 235436.
7. S. Ali, V. S. Myasnichenko and E. C. Neyts, *Physical Chemistry Chemical Physics*, 2016, 18, 792-800.
8. D. Liu, J. Lian and Q. Jiang, *The Journal of Physical Chemistry C*, 2009, 113, 1168-1170.
9. A. S. Barnard and L. A. Curtiss, *ChemPhysChem*, 2006, 7, 1544-1553.
10. L. F. Oliveira, N. Tarrat, J. Cuny, J. Morillo, D. Lemoine, F. Spiegelman and M. Rapacioli, *The Journal of Physical Chemistry A*, 2016, 120, 8469-8483.
11. I. K. Suh, H. Ohta and Y. Waseda, *Journal of Materials Science*, 1988, 23, 757-760.
12. T. Hiemstra, *Geochimica et Cosmochimica Acta*, 2015, 158, 179-198.
13. W. R. Tyson and W. A. Miller, *Surface Science*, 1977, 62, 267-276.
14. T. Dubberstein and H. P. Heller, *High Temperatures-High Pressures*, 2015, 44, 393-406.
15. I. Egry, G. Lohoefer, E. Schwartz, J. Szekely and P. Neuhaus, *Metallurgical and Materials Transactions B*, 1998, 29, 1031-1035.
16. R. Novakovic, E. Ricci, F. Gnecco, D. Giuranno and G. Borzone, *Surface science*, 2005, 599, 230-247.
17. J. Lee, W. Shimoda and T. Tanaka, *Materials transactions*, 2004, 45, 2864-2870.
18. R. Novakovic, E. Ricci, D. Giuranno and A. Passerone, *Surface science*, 2005, 576, 175-187.
19. S. Ozawa, K. Morohoshi, T. Hibiya and H. Fukuyama, *Journal of Applied Physics*, 2010, 107, 014910.